

Supporting Information

Stable and wide-wavelength tunable luminescence of CsPbX₃ nanocrystals encapsulated in metal-organic frameworks

Hailong Wu, Lijia Yao, Wenqian Cao, Yu Yang, Yuanjing Cui*, Deren Yang and Guodong

Qian*

State Key Laboratory of Silicon Materials, Cyrus Tang Center for Sensor Materials and
Applications, School of Materials Science and Engineering, Zhejiang University, Hangzhou

310027, China. E-mail: cuiyj@zju.edu.cn, gdqian@zju.edu.cn

1. Experimental section

1.1 Chemicals and materials

Cesium carbonate (Cs_2CO_3 , 99.9%), lead nitrate ($\text{Pb}(\text{NO}_3)_2$, 99.0%), cesium chloride (CsCl , 99.99%), cesium bromide (CsBr , 99.99%), cesium iodide (CsI , 99.99%), indium chloride tetrahydrate ($\text{InCl}_3 \cdot 4\text{H}_2\text{O}$, 99.99%), 1,3,5-tri(4-carboxyphenyl)benzene (H_3BTB , 98%), organic dyes and other reagents were commercially available and used without further purification.

1.2 Synthesis of ZJU-28 crystals

The ZJU-28 crystals were synthesized according to our previous work with minor modification.¹ $\text{InCl}_3 \cdot 4\text{H}_2\text{O}$ (176mg, 0.6mmol) and H_3BTB (133mg, 0.3mmol) were dissolved in the solution of N, N-dimethylformamide (9 mL), 1,4-dioxane (6mL), H_2O (1mL) and nitric acid (63mL). The resultant solution was sealed in a Teflon-lined stainless-steel bomb at 130 °C for 24h. After cooling to room temperature, colorless ZJU-28 crystals of needle-like morphology were collected by filtration, washed with DMF and dried in air.

1.3 Synthesis of ZJU-28 \supset CsPbX₃ crystals

ZJU-28 \supset CsPbX₃ crystals were synthesized via the sequential deposition method. The fresh ZJU-28 crystals (15 mg) were firstly immersed in 10 mL $\text{Pb}(\text{NO}_3)_2$ DMF solution (0.05 mol/L) at 60 °C for 1h. The ZJU-28 \supset Pb²⁺ crystals were collected by filtration and washed three times each with DMF and ethanol. After drying in the air, ZJU-28 \supset Pb²⁺ crystals were then added in 5mL CsX methanol solution (0.1mol/L) for about 12h. Finally, the ZJU-28 \supset CsPbX₃ crystals were collected by filtration, washed with ethanol for rinsing the perovskite microcrystals on the surface of ZJU-28 crystals and dried in air. The composition of internal CsPbX₃ NCs of ZJU-

$28\text{-}\text{CsPbX}_3$ crystals can be tuned by simply adjusting the halide stoichiometry of the CsX methanol solution. In details, ZJU- $28\text{-}\text{CsPbBr}_3$ crystals were obtained as CsBr methanol solution is used, and ZJU- $28\text{-}\text{CsPbCl}_x\text{Br}_{3-x}$ ($x = 0, 1, 1.5, 2$) and ZJU- $28\text{-}\text{CsPbBr}_{3-y}\text{I}_y$ ($y = 1, 1.5, 2$) crystals were prepared by gradually replacing the Br with Cl and I in the CsX methanol solution respectively.

1.4 Synthesis of CsPbX_3 NCs

CsPbX_3 NCs were synthesized via typical hot-injection technique reported by Protesescu et al.² Firstly, Cs_2CO_3 (0.814 g), octadecene (40 mL) and oleic acid (2.5 mL) were loaded into 100mL 3-neck flask, dried for 1 h at 120 °C and then heated to 150 °C under N_2 for 1 h to prepare Cs-oleate. Octadecene (10 mL) and PbX_2 (0.376 mmol) were added in 50 mL 3-neck flask and dried at 120 °C for 1 h, following by injection of dried oleyl amine (1 mL) and oleic acid (1 mL). After complete solubilization of PbX_2 salt, the temperature was raised to 160 °C and then the prepared Cs-oleate (1.25 mL) was swiftly injected. About 5 ~ 10 s later, the reaction was stopped by ice-water bath. Finally, the crude solution was transferred to a centrifuge tube and purified by centrifugation at 15000 rpm for 10 min. After the supernatant was discarded, the CsPbX_3 NCs were redispersed in toluene for further study.

1.5 Measurements

Powder X-ray diffraction (PXRD) patterns were collected on an X'Pert PRO diffractometer with Cu $\text{K}\alpha$ radiation ($\lambda = 1.542 \text{ \AA}$) at room temperature, in the range of $2\theta = 5\text{-}50^\circ$. The X-ray photoelectron spectroscopy (XPS) was collected on a Thermo Scientific K-Alpha+ spectrometer. The morphology and energy dispersive spectrometry (EDS) results were detected with a field-emission scanning electron microscopy (FE-SEM, Hitachi S4800). The TEM and

HR-TEM images were taken with a FEI Tecnai G2 F20 S-TWIN which operated at an acceleration voltage of 200 KV. UV-vis absorption spectroscopy was measured with UV-2600 UV-vis spectrophotometer (Shimadzu, Japan). The one-photon excited fluorescence spectra were obtained on a Hitachi F-4600 fluorescence spectrometer at room temperature. The time-resolved PL decay and the quantum yields were all recorded on an Edinburgh Instrument F920 spectrometer. The microscopy images of ZJU-28 \rightarrow CsPbX₃ crystals were captured on an Olympus IX 71 inverted fluorescent microscope and the corresponding emission spectra were recorded by the fiber optic spectrometer (PG2000-Pro, Ideaoptics Instruments). For the measurement of 2PE luminescence, an optical parametric amplifier (Spirit-OPA + Spirit-OPA-UV3, Newport Corporation) was pumped by a fully automated ultrafast laser system (Spirit One 1040-8, 8 W at 1040 nm, Newport Corporation), which was used for generating the excitation pulse (200 kHz, 780-980 nm, pulse width < 400 fs). The incident laser was coupled to the microscope (IX71, Olympus), focusing on crystals through an objective lens (Olympus LUCPlanFL N 10 \times , numerical aperture = 0.40). The emission was then focused and collected by the fiber optic spectrometer (PG2000-Pro, Ideaoptics Instruments). More details of the experiment setup and the test light path are shown in Figure S22.

2. Analysis

2.1 Determination of concentrations of CsPbX₃ NCs dispersed in toluene

As for the concentration of colloidal CsPbX₃ NCs (X₃ = ClBr₂, Br₃, and BrI₂) dispersed in toluene, 20 mg CsPbX₃ NCs were weighed and dispersed into 5 ml toluene for dilute solution. The mass of weighed CsPbX₃ NCs and the volume of toluene solution are denoted as m_{X₃} and

V_s , respectively. The molecular weights (M_{X_3}) of CsPbClBr₂ NCs, CsPbBr₃ NCs and CsPbBrI₂ NCs are 535.35 g/mol, 579.80 g/mol and 674.00 g/mol, respectively. The particle volume V_{X_3} can be estimated from TEM analyses that all of their morphology approximates cubic with average particle sizes of 9.20 nm, 9.27 nm and 11.3 nm for CsPbClBr₂ NCs, CsPbBr₃ NCs and CsPbBrI₂ NCs, respectively. The unit cell volume (V_{UX_3}) of CsPbX₃ NCs can be calculated from the spacing of specific crystal planes in TEM analysis. Therefore, the molar concentration of colloidal CsPbX₃ NCs dispersed in toluene can be expressed to be $C_{X_3} = (m_{X_3}/M_{X_3})(V_{UX_3}/V_{X_3})(1/V_s)$, and $C_{ClBr_2} = 1.60 \mu\text{M}$, $C_{Br_3} = 1.69 \mu\text{M}$ and $C_{BrI_2} = 0.98 \mu\text{M}$ can be calculated.

2.2 Determination of concentrations of CsPbX₃ NCs in ZJU-28 \Rightarrow CsPbX₃ crystals

The molar concentration of the CsPbX₃ NCs ($X_3 = \text{ClBr}_2, \text{Br}_3, \text{and BrI}_2$) encapsulated in ZJU-28 crystals is calculated based on the data of element mapping. Because the ZJU-28 frameworks are anionic, cations such as Cs⁺ and Pb²⁺ are easier to enter into the channels of ZJU-28 than anions such as X⁻ during the in-situ growth of CsPbX₃ NCs, resulting in excess cations in ZJU-28 crystals. We assume that all halogen ions are derived from the internal CsPbX₃ NCs and all indium ions derived from ZJU-28 crystals. Therefore, the ratio of the number of CsPbX₃ to the number of indium ions is $n_{X_3}/(3 \times n_{In})$, where n_{X_3} represents the atomic percentage of halogen ions ($n_{Cl} + n_{Br}$ for CsPbClBr₂, n_{Br} for CsPbBr₃ and $n_{Br} + n_{I}$ for CsPbBrI₂) and n_{In} represents the atomic percentage of indium ions. The unit cell of ZJU-28 contains 6 indium ions with a unit cell volume V_{ZU} of 10.61629 nm³ according to the CIF files of ZJU-28. A CsPbX₃ unit cell contains one CsPbX₃ molecule and its volume (V_{UX_3}) can be obtained by the method mentioned above. The internal CsPbX₃ NCs can be approximately spherical with

average particle diameter of 8.33 nm for ZJU-28 \supset CsPbClBr₂, 9.09 nm for ZJU-28 \supset CsPbBr₃ and 12.5 nm for ZJU-28 \supset CsPbBrI₂, and thus the particle volume V_{X3} can be estimated. Therefore, the molar concentration of the CsPbX₃ NCs in ZJU-28 crystals can be expressed to be $C_{ZX3} = (2 \times n_{X3} / n_{In}) (V_{UX3} / V_{X3}) [1 / (N_A \cdot V_{ZU})]$, and $C_{ZClBr2} = 138 \mu\text{M}$, $C_{Br3} = 111 \mu\text{M}$ and $C_{ZBrI2} = 39 \mu\text{M}$ can be calculated.

2.3 Determination of two-photon action cross-section of ZJU-28 \supset CsPbX₃ crystals

Two-photon action cross-section of ZJU-28 \supset CsPbX₃ crystals were evaluated via the 2PE luminescence reference method.^{3, 4} The intensity of the two-photon excited fluorescence (TPEF) is given by equation S1:

$$A_{TPEF} = cI^2n^2\sigma_2\eta F_{col} \quad (\text{S1})$$

Where c , I , n , σ_2 , η and F_{col} represent the molar concentration, exciting laser intensity, refractive index, the two-photon absorption cross-section, fluorescence quantum yield, and a phenomenological collection factor, respectively.

In the standard 2PA luminescence reference method, this measurement is carried out in a relative way: the two-photon action cross-section of sample at every wavelength in the investigated range is determined by comparison of 2PE luminescence intensity of the sample with that of a reference for which the wavelength dependence of the two-photon absorption cross-section σ_{2ref} and quantum yield η_{ref} is precisely known.

$$\frac{A_s}{A_{ref}} = \frac{c_s I^2 n^2 \sigma_{2s} \eta_s F_{col}}{c_{ref} I^2 n^2 \sigma_{2ref} \eta_{ref} F_{col}} \quad (\text{S2})$$

Where c_s , σ_{2s} and η_s represent the molar concentration, the two-photon absorption cross-section, quantum yield of sample respectively, while c_{ref} , σ_{2ref} and η_{ref} represent the molar concentration, the two-photon absorption cross-section, quantum yield of the reference respectively.

The phenomenological collection factor F_{col} is a parameter about experiment setup, that is, optical path, sensitivity of the detector, apertures, collection angle. The intensity of the laser radiation I and the collection factor F_{col} are cancelled considering that the experimental conditions are the same. Similarly, the refractive index of the reference and the sample can be also cancelled if they are close. Therefore, the two-photon action cross-section of sample can be calculated by equation S3:

$$\eta_s \sigma_{2s} = \left(\frac{A_s}{A_{ref}}\right) \left(\frac{c_{ref}}{c_s}\right) \eta_{ref} \sigma_{2ref} \quad (S3)$$

We chose standard dyes Coumarin 153 (C153), Rhodamine 6G and Rhodamine B as the reference for ZJU-28 \supset CsPbClBr₂, ZJU-28 \supset CsPbBr₃ and ZJU-28 \supset CsPbBrI₂ crystals respectively, because their emission peak positions are close to these of the corresponding samples and their two-photon absorption cross-section and quantum yield have been reported. The quantum yield of C153 with a concentration of 10⁻⁵ M in cyclohexane is 90%,⁵ and it possesses a two-photon absorption cross-section of 32 GM (32 \times 10⁻⁵⁰ cm⁴·s·photon⁻¹) at 780 nm;⁶ Two-photon absorption cross-section of Rhodamine 6G is 56 GM (11 \times 10⁻⁵⁰ cm⁴·s·photon⁻¹) at 780 nm and its quantum yield at 10⁻⁴ M (ethanol solution) is 89.5%.^{6, 7} Rhodamine B ethanol solution with concentration of 10⁻⁵ M shows a quantum efficiency of 67% and two-photon absorption cross-section of 14 GM (14 \times 10⁻⁵⁰ cm⁴·s·photon⁻¹) at 980 m.^{6, 8} The two-photon action cross-sections of the synthesized ZJU-28 \supset CsPbClBr₂ crystals and ZJU-28 \supset CsPbBr₃ crystals and ZJU-28 \supset CsPbBrI₂ crystals are thus calculated to be 8.66 \times 10⁴ GM (at 780 nm), 1.58 \times 10⁶ GM (at 780 nm) and 1.96 \times 10⁵ GM (at 980 nm), respectively. In addition, as a comparison, the two-photon action cross-section of the synthesized CsPbClBr₂ NCs, CsPbBr₃ NCs and CsPbBrI₂ NCs are also calculated to be 8.93 \times 10⁴ GM, 1.45 \times 10⁶ GM and

2.43×10^5 GM at corresponding wavelength, respectively.

3. Supporting Tables and Figures

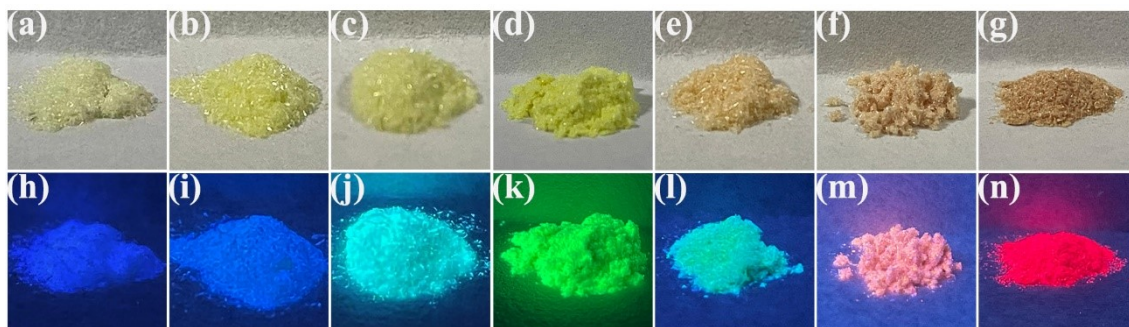


Fig. S1. Photographs of ZJU-28 CsPbX_3 ($X_3 = \text{Cl}_2\text{Br}$, $\text{Cl}_{1.5}\text{Br}_{1.5}$, ClBr_2 , Br_3 , Br_2I , $\text{Br}_{1.5}\text{I}_{1.5}$, BrI_2 , from left to right) crystals under day light (a-g) and UV light (h-n).



Fig. S2. Photographs of CsPbX_3 NCs ($X_3 = \text{Cl}_2\text{Br}$, $\text{Cl}_{1.5}\text{Br}_{1.5}$, ClBr_2 , Br_3 , Br_2I , $\text{Br}_{1.5}\text{I}_{1.5}$, BrI_2 , from left to right) dispersed in toluene under (a) day light and (b) UV light.

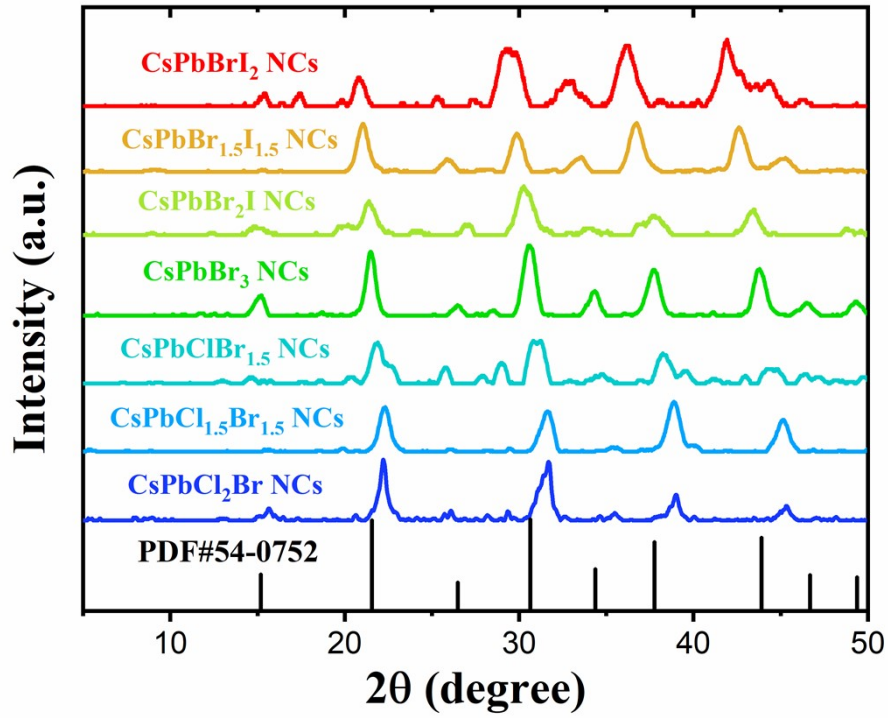


Fig. S3. PXRD patterns of the synthesized CsPbX₃ NCs.

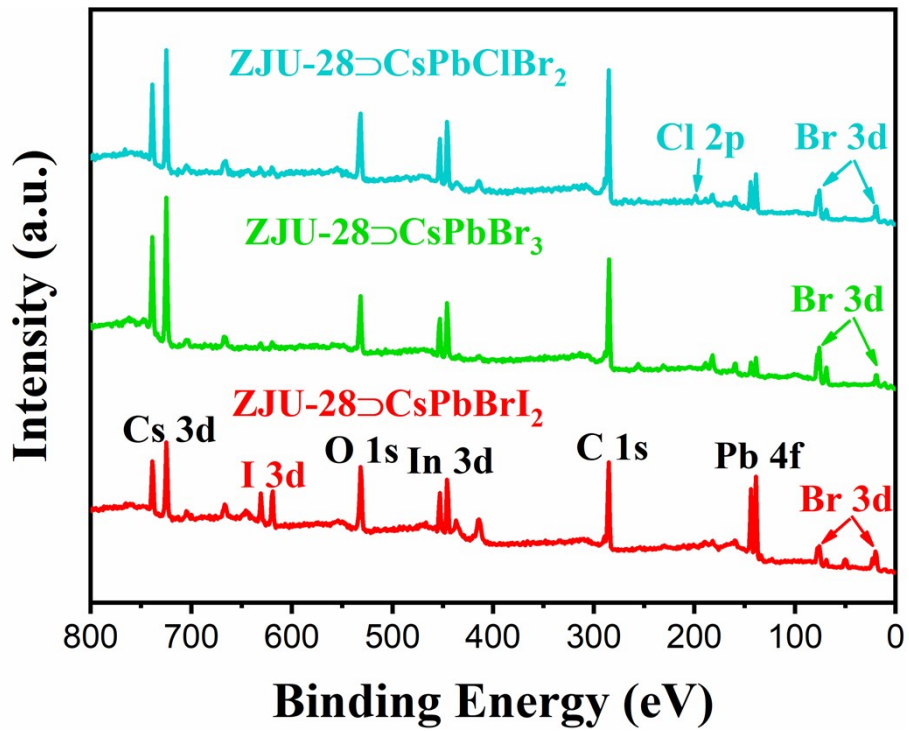


Fig. S4. XPS patterns of ZJU-28@CsPbClBr₂, ZJU-28@CsPbBr₃, and ZJU-28@CsPbBrI₂

crystals.

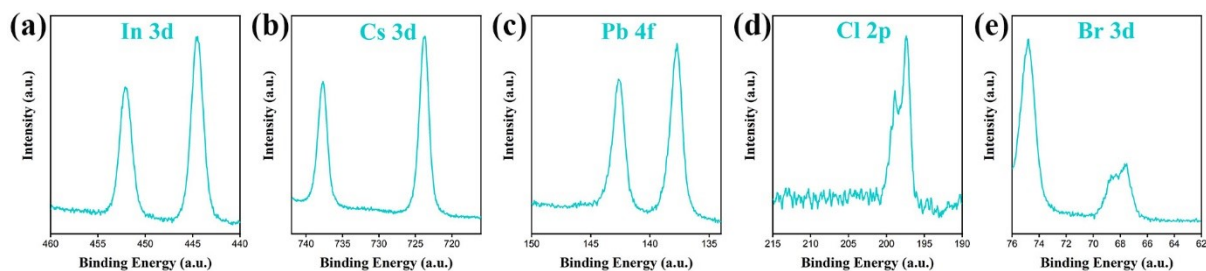


Fig. S5. High resolution XPS spectra of (a) In 3d, (b) Cs 3d, (c) Pb 4f, (d) Cl 2p and (e) Br 3d of ZJU-28∩CsPbClBr₂ crystals.

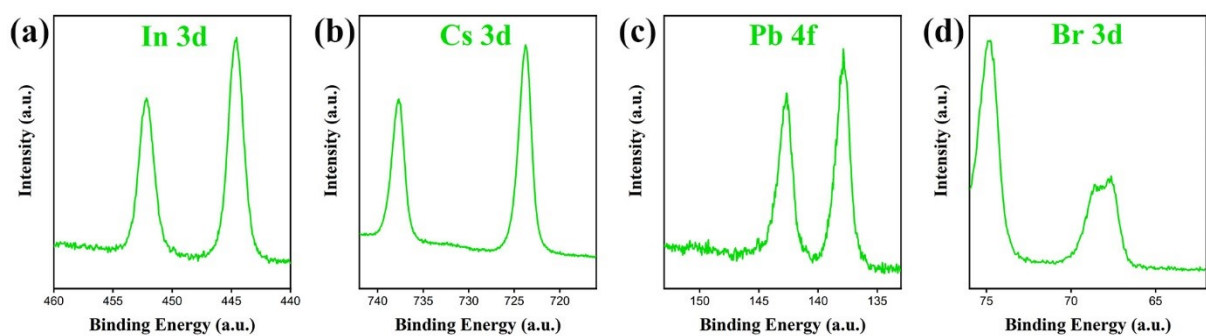


Fig. S6. High resolution XPS spectra of (a) In 3d, (b) Cs 3d, (c) Pb 4f and (d) Br 3d of ZJU-28∩CsPbBr₃ crystals.

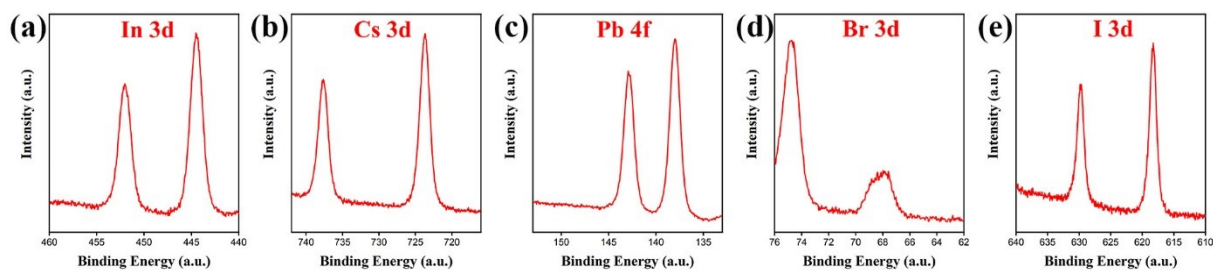


Fig. S7. High resolution XPS spectra of (a) In 3d, (b) Cs 3d, (c) Pb 4f, (d) Br 3d and (e) I 3d of ZJU-28∩CsPbBrI₂ crystals

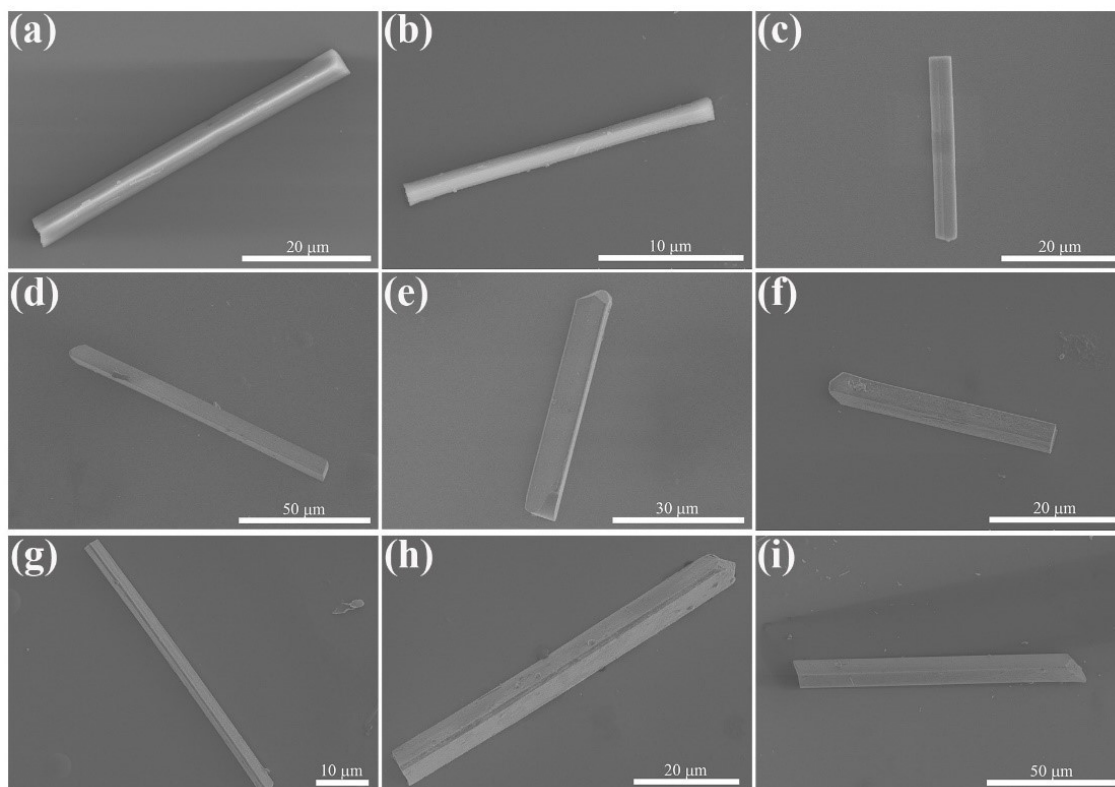


Fig. S8. The SEM images of a (a) ZJU-28, (b) ZJU-28 \supset Pb²⁺, (c) ZJU-28 \supset CsPbCl₂Br, (d) ZJU-28 \supset CsPbCl_{1.5}Br_{1.5}, (e) ZJU-28 \supset CsPbClBr₂, (f) ZJU-28 \supset CsPbBr₃, (g) ZJU-28 \supset CsPbBr₂I, (h) ZJU-28 \supset CsPbBr_{1.5}I_{1.5} and (i) ZJU-28 \supset CsPbBrI₂ single crystal.

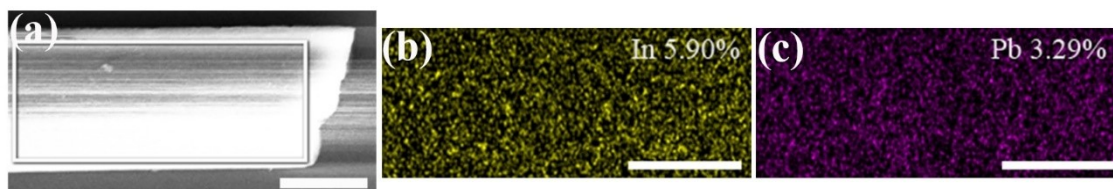


Fig. S9. (a) Selected SEM image of ZJU-28 \supset Pb²⁺ and the corresponding elemental mapping diagrams of (b) In and (c) Pb. Scale bar, 5 μ m.

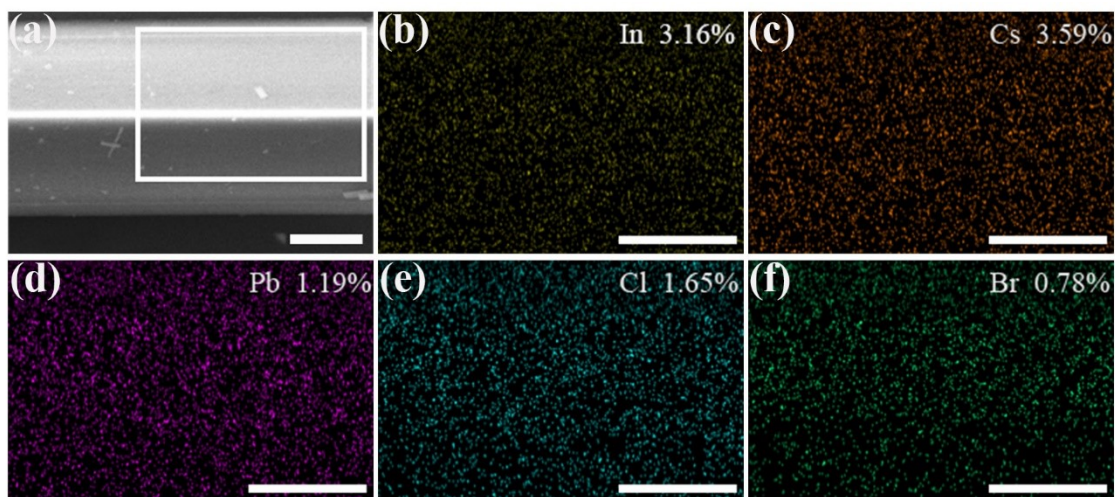


Fig. S10. (a) Selected SEM image of ZJU-28 \supset CsPbCl₂Br and the corresponding elemental mapping diagrams of (b) In, (c) Cs, (d) Pb, (e) Cl and (f) Br. Scale bar, 5 μ m.

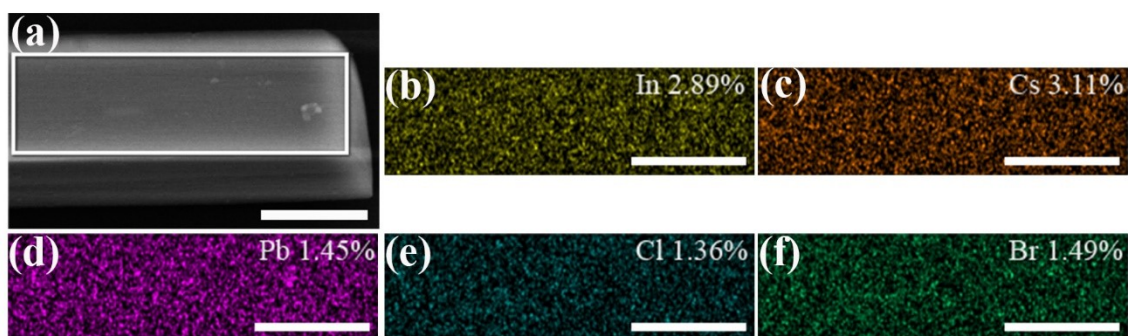


Fig. S11. (a) Selected SEM image of ZJU-28 \supset CsPbCl_{1.5}Br_{1.5} and the corresponding elemental mapping diagrams of (b) In, (c) Cs, (d) Pb, (e) Cl and (f) Br. Scale bar, 5 μ m.

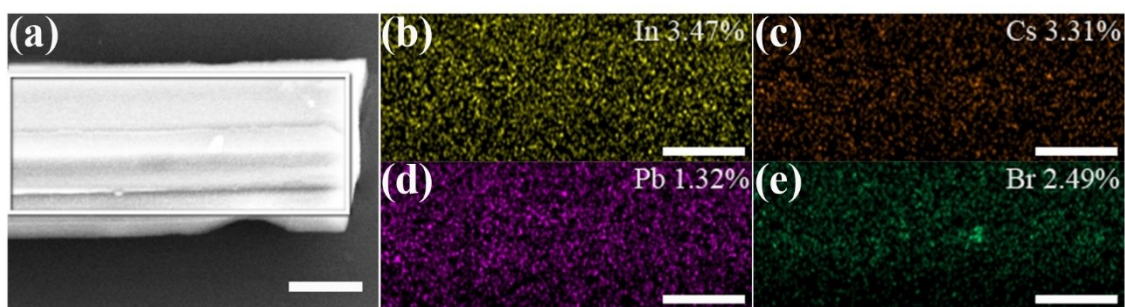


Fig. S12. (a) Selected SEM image of ZJU-28-CSPbBr₃ and the corresponding elemental mapping diagrams of (b) In, (c) Cs, (d) Pb and (e) Br. Scale bar, 5 μm.

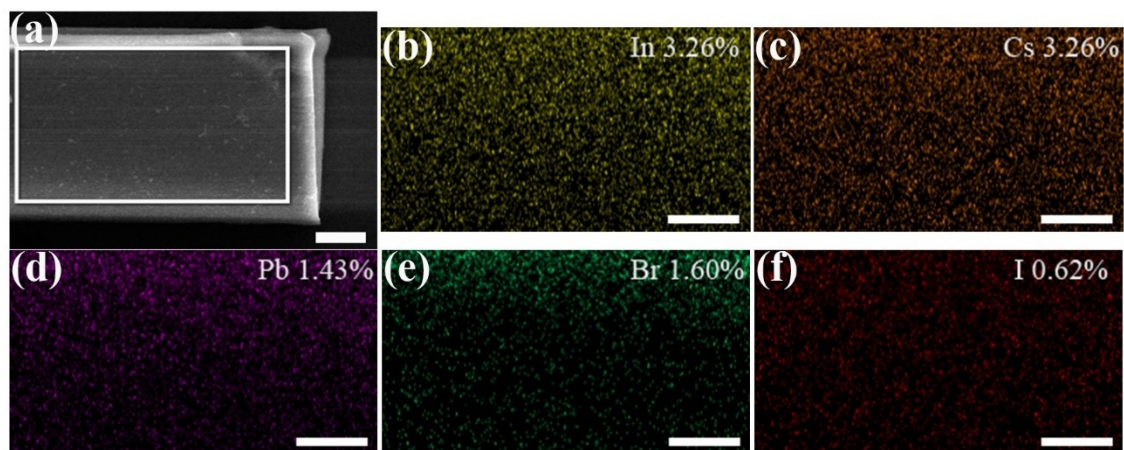


Fig. S13. (a) Selected SEM image of ZJU-28-CSPbBr₂I and the corresponding elemental mapping diagrams of (b) In, (c) Cs, (d) Pb, (e) Br and (f) I. Scale bar, 5 μm.

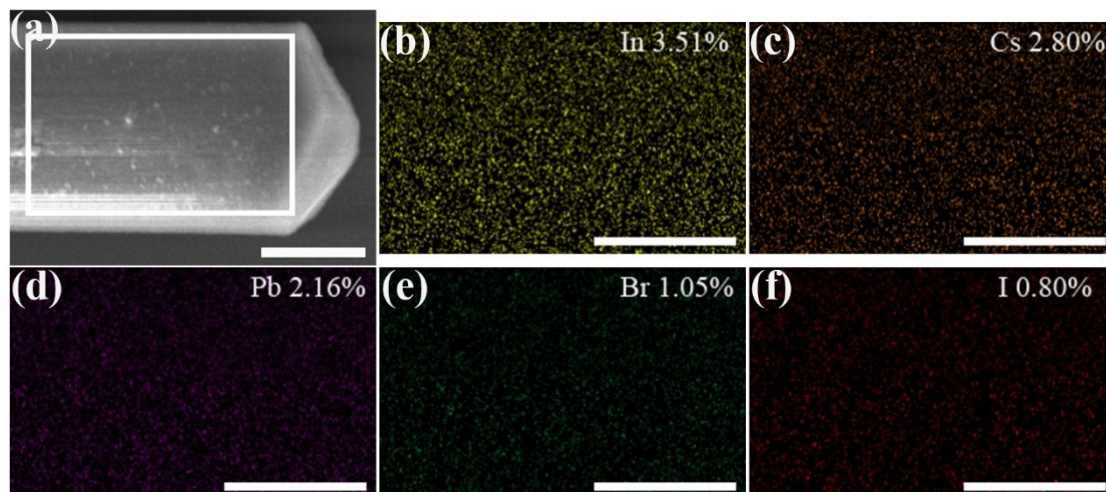


Fig. S14. (a) Selected SEM image of ZJU-28 \supset CsPbBr_{1.5}I_{1.5} and the corresponding elemental mapping diagrams of (b) In, (c) Cs, (d) Pb, (e) Br and (f) I. Scale bar, 5 μ m.

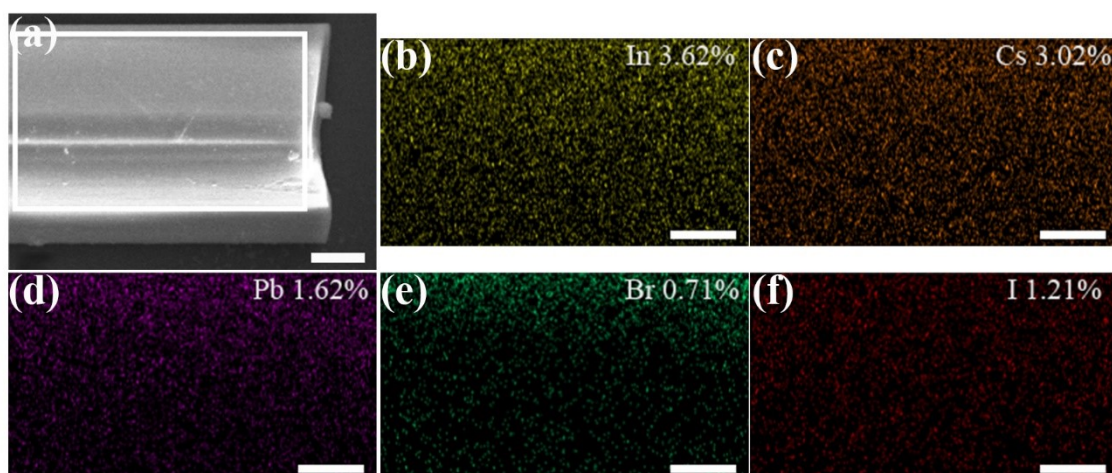


Fig. S15. (a) Selected SEM image of ZJU-28 \supset CsPbBrI₂ and the corresponding elemental mapping diagrams of (b) In, (c) Cs, (d) Pb, (e) Br and (f) I. Scale bar, 5 μ m.

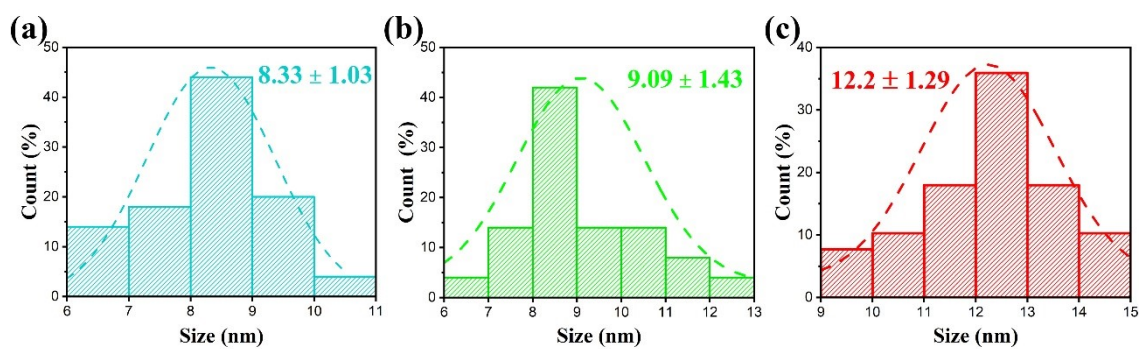


Fig. S16. Particle size distribution histograms of perovskite NCs encapsulated in (a) ZJU-28 \supset CsPbClBr₂, (b) ZJU-28 \supset CsPbBr₃, and (c) ZJU-28 \supset CsPbBrI₂, respectively.

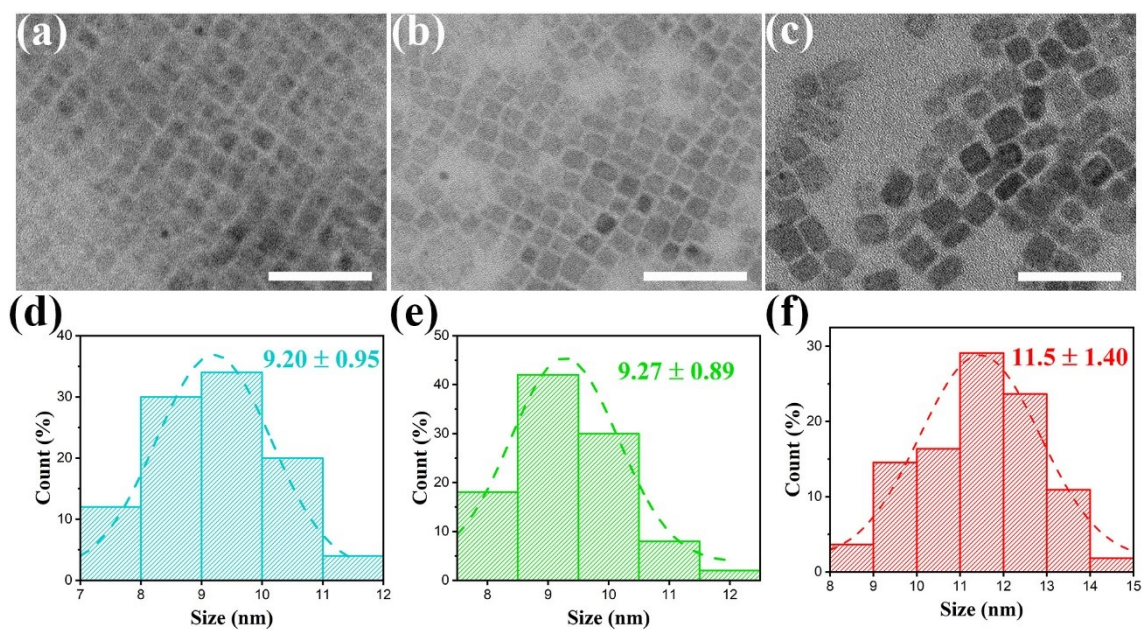


Fig. S17. TEM images and particle size distribution histograms of (a, d) CsPbClBr₂ NCs, (b, e) CsPbBr₃ NCs, and (c, f) CsPbBrI₂ NCs respectively. Scale bar, 50 nm.

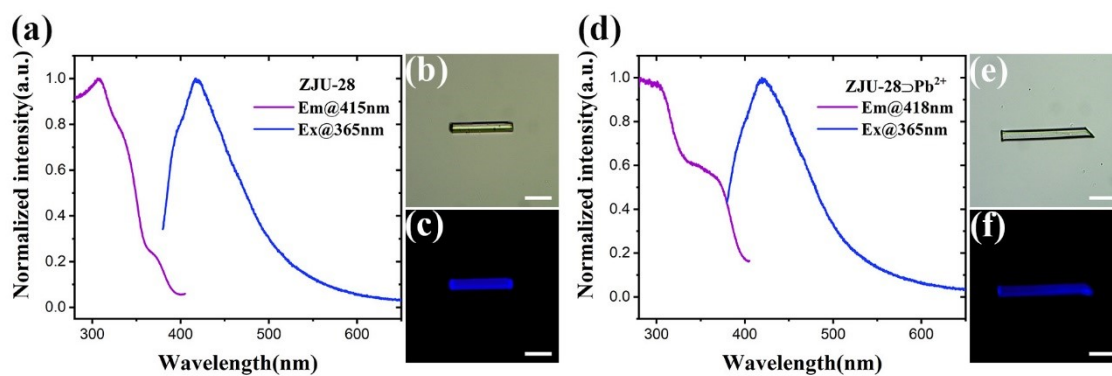


Fig. S18. (a) Excitation and emission spectra of ZJU-28 crystals. The microscopy images of an isolated ZJU-28 microcrystal under (b) day light and (c) UV light. (d) Excitation and emission spectra of ZJU-28-Pb²⁺ crystals. The microscopy images of an isolated ZJU-28-Pb²⁺ microcrystal under (e) day light and (f) UV light. Scale bar, 50 μm.

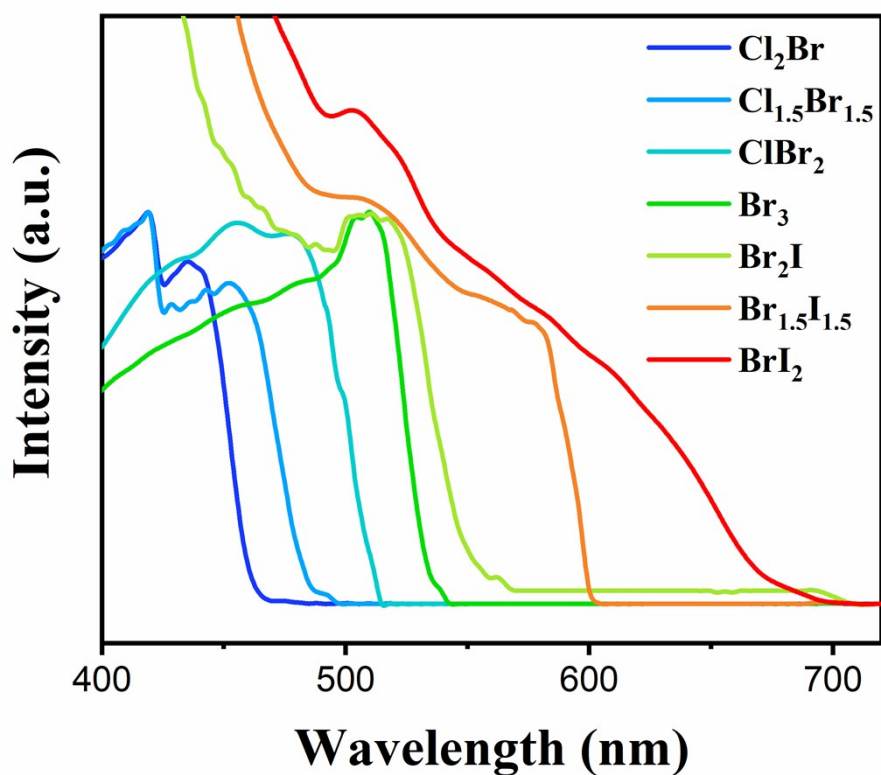


Fig. S19. Absorption spectra of ZJU-28 CsPbX_3 crystals.

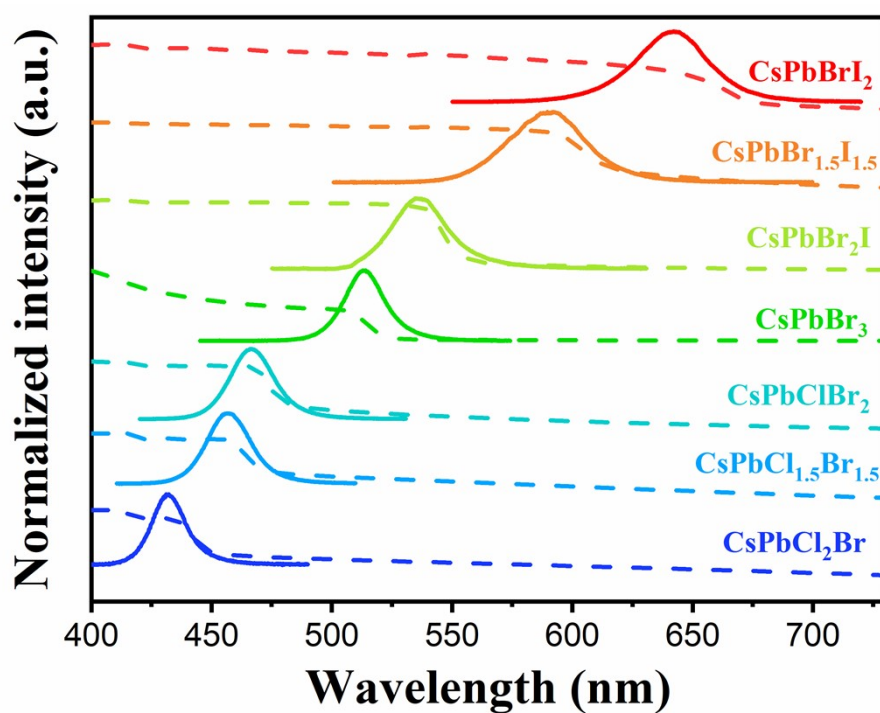


Fig. S20. Absorbance (dashed lines) and PL (solid lines) spectra of the CsPbX_3 NCs dispersed in toluene.

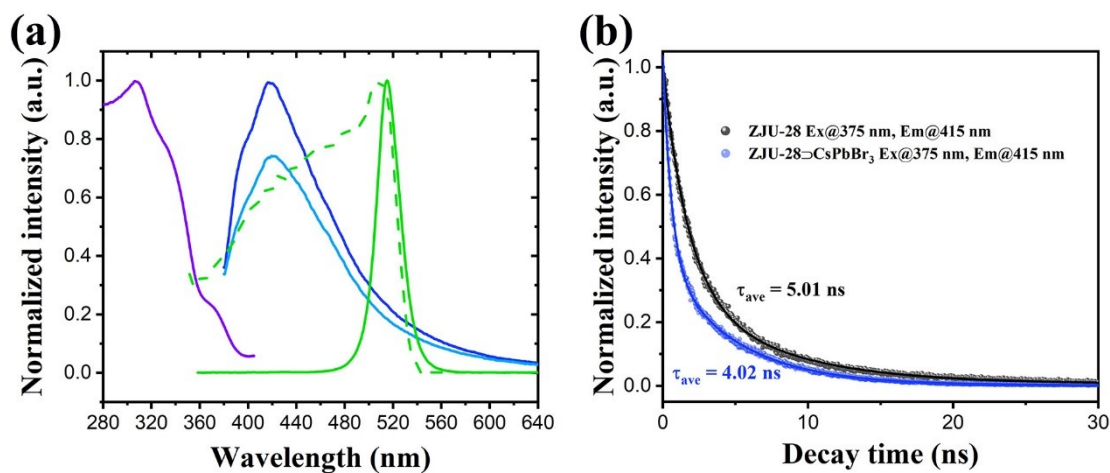


Fig. S21. (a) Excitation (purple) and emission (blue) spectra of ZJU-28, emission spectra (skyblue) of ZJU-28 \rightarrow Pb²⁺, and the absorbance (dashed green) and PL (solid green) spectra of ZJU-28 \rightarrow CsPbBr₃. (b) Time-resolved PL decays of ZJU-28 and ZJU-28 \rightarrow CsPbX₃ crystals

Table S1. optical properties of ZJU-28 \rightarrow CsPbX₃ crystals and corresponding colloidal perovskite NCs.

Samples (Corresponding NCs)	Emission Wavelength (nm)	Emission FWHM (nm)	Quantum efficient (%)
ZJU-28 \rightarrow CsPbCl ₂ Br (CsPbCl ₂ Br NCs)	450 (432)	21.3 (16.4)	2.45 (11)
ZJU-28 \rightarrow CsPbCl _{1.5} Br _{1.5} (CsPbCl _{1.5} Br _{1.5} NCs)	470 (456)	31.3 (21.3)	7.76 (26)
ZJU-28 \rightarrow CsPbClBr ₂ (CsPbClBr ₂ NCs)	491 (467)	25.7 (21.3)	19.8 (32)
ZJU-28 \rightarrow CsPbBr ₃ (CsPbBr ₃ NCs)	515 (513)	22.3 (19.3)	27.0 (62)
ZJU-28 \rightarrow CsPbBr ₂ I (CsPbBr ₂ I NCs)	542 (535)	25.0 (26.9)	5.56 (53)
ZJU-28 \rightarrow CsPbBr _{1.5} I _{1.5} (CsPbBr _{1.5} I _{1.5} NCs)	593 (592)	34.5 (37.3)	13.2 (61)
ZJU-28 \rightarrow CsPbBrI ₂ (CsPbBrI ₂ NCs)	661 (642)	35.4 (34.7)	19.1 (78)

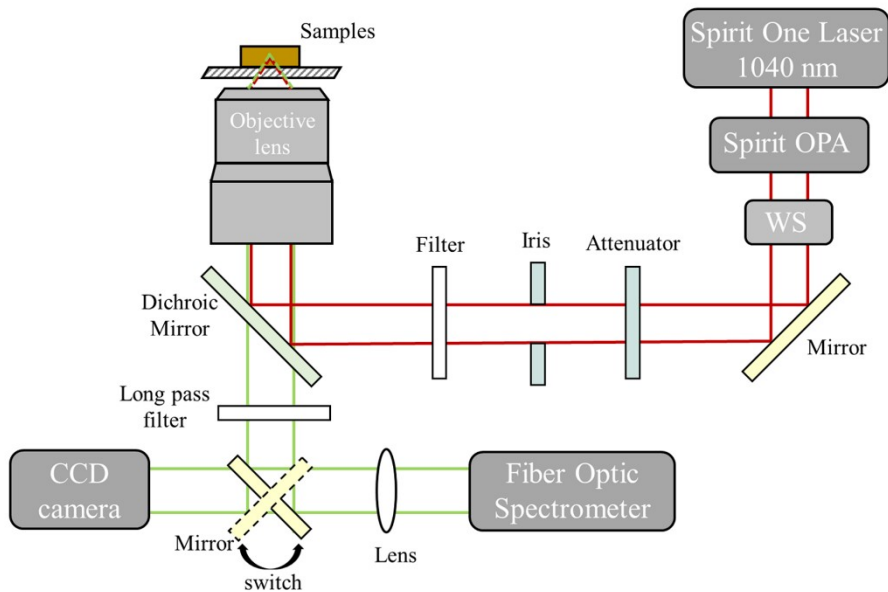


Fig. S22. Schematic diagram of the experimental setup for measuring 2PE luminescence. OPA and WS are short for optical parametric amplifier and wavelength separators, respectively.

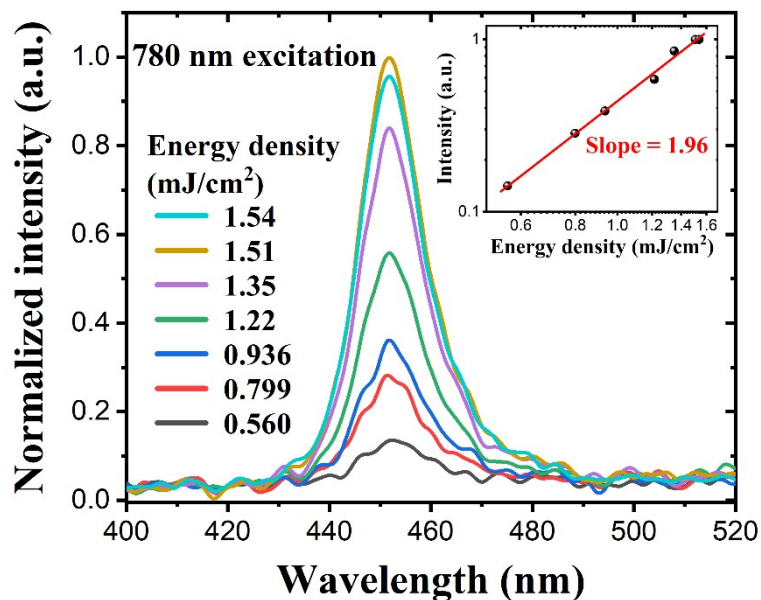


Fig. S23. 2PE luminescence of an isolated ZJU-28 CsPbCl₂Br microcrystal under 780 nm fs laser excitation. Inset displays emission intensity as a function of pump energy density showing the slope of 1.96. Test environment: temperature of 25 °C, humidity of 55%.

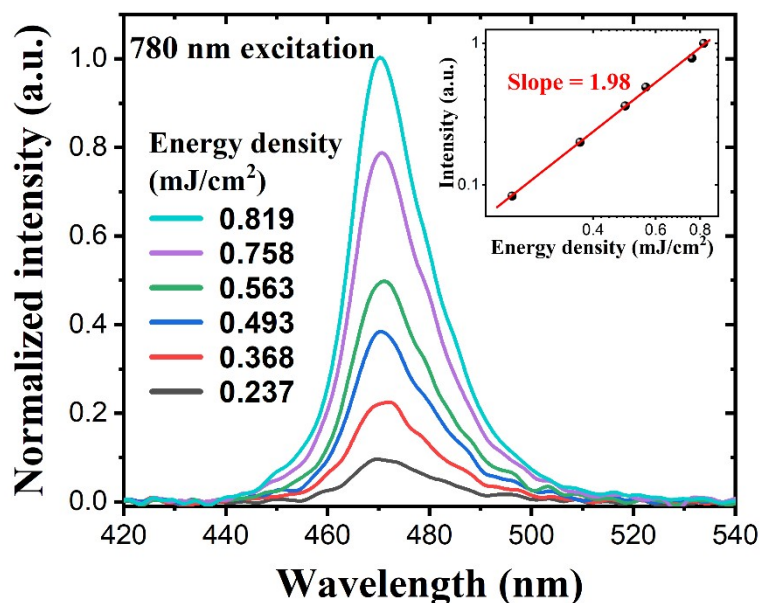


Fig. S24. 2PE luminescence of an isolated ZJU-28 \supset CsPbCl_{1.5}Br_{1.5} microcrystal under 780 nm fs laser excitation. Inset displays emission intensity as a function of pump energy density showing the slope of 1.98. Test environment: temperature of 25 °C, humidity of 55%.

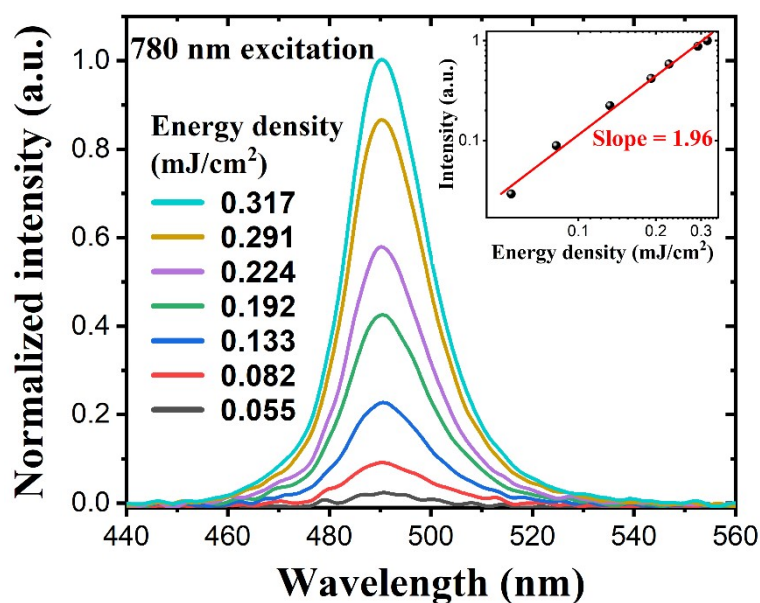


Fig. S25. 2PE luminescence of an isolated ZJU-28 \supset CsPbClBr₂ microcrystal under 780 nm fs laser excitation. Inset displays emission intensity as a function of pump energy density showing the slope of 1.96. Test environment: temperature of 25 °C, humidity of 55%.

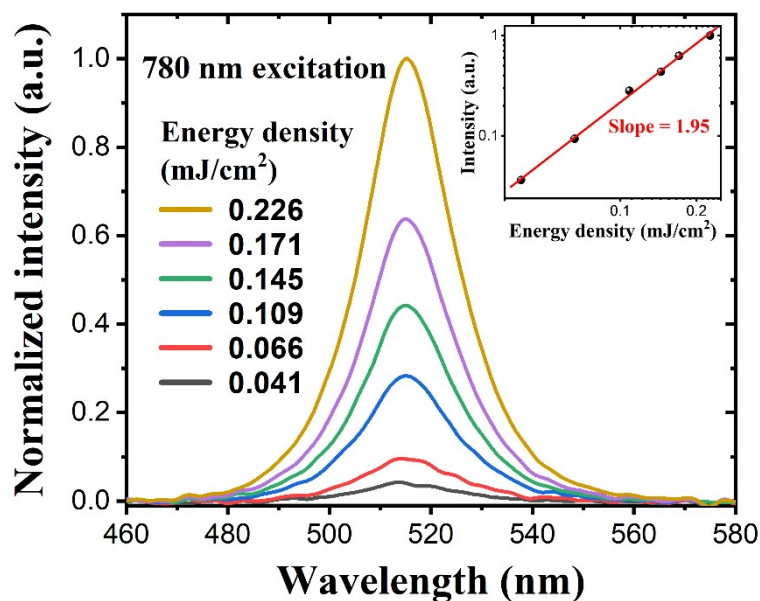


Fig. S26. 2PE luminescence of an isolated ZJU-28 CsPbBr₃ microcrystal under 780 nm fs laser excitation. Inset displays emission intensity as a function of pump energy density showing the slope of 1.95. Test environment: temperature of 25 °C, humidity of 55%.

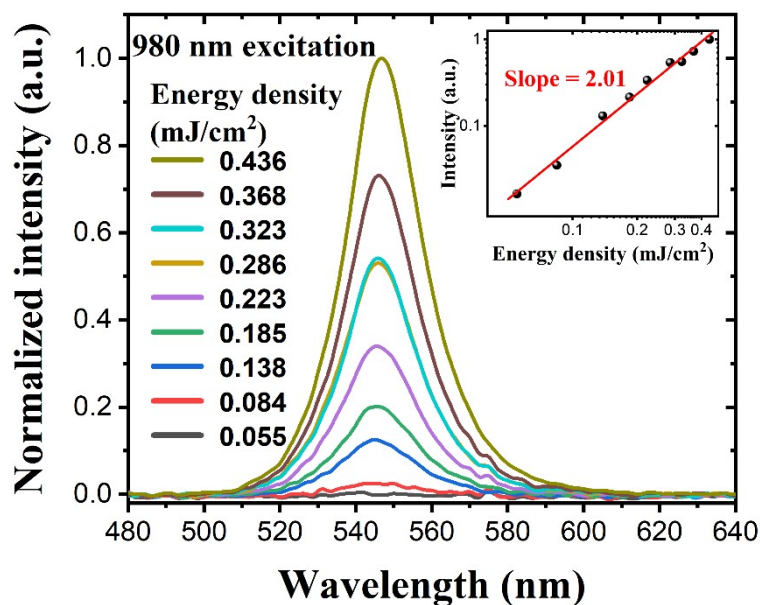


Fig. S27. 2PE luminescence of an isolated ZJU-28 CsPbBr₂I microcrystal under 980 nm fs laser excitation. Inset displays emission intensity as a function of pump energy density showing the slope of 2.01. Test environment: temperature of 25 °C, humidity of 55%.

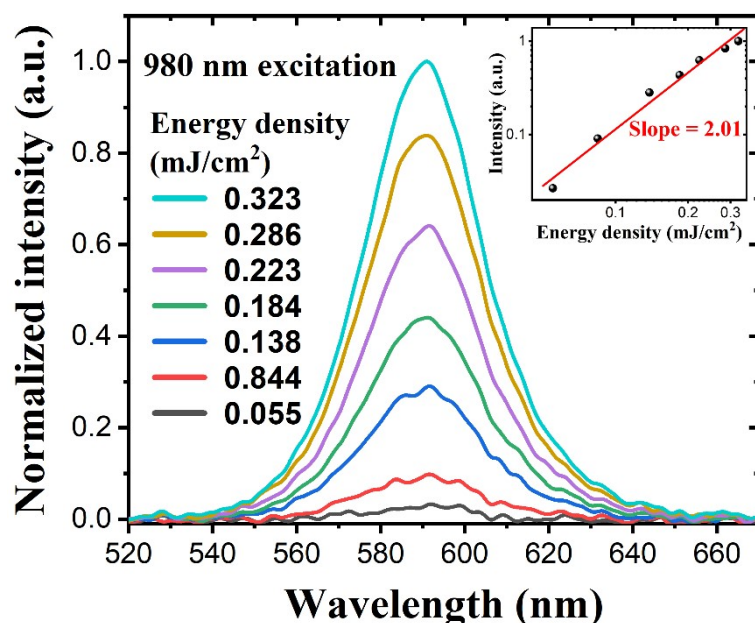


Fig. S28. 2PE luminescence of an isolated ZJU-28 \supset CsPbBr_{1.5}I_{1.5} microcrystal under 980 nm fs laser excitation. Inset displays emission intensity as a function of pump energy density showing the slope of 2.01. Test environment: temperature of 25 °C, humidity of 55%.

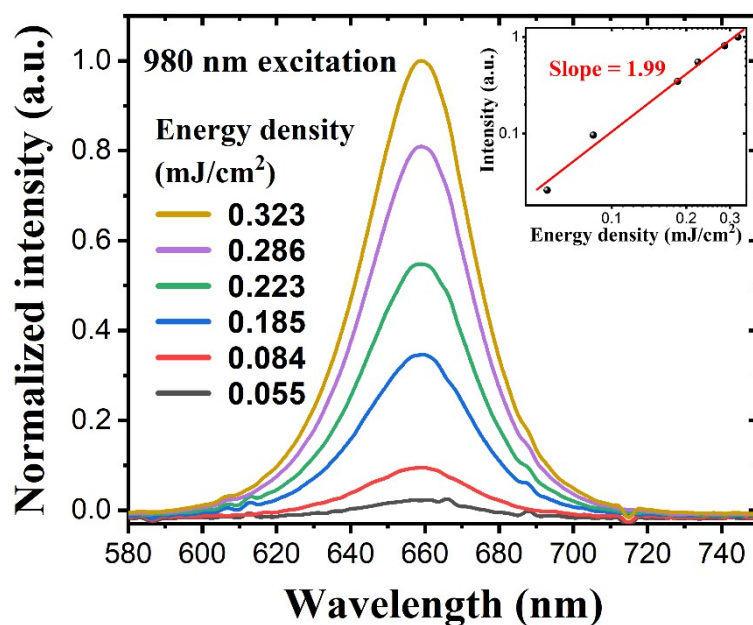


Fig. S29. 2PE luminescence of an isolated ZJU-28 \supset CsPbBrI₂ microcrystal under 980 nm fs laser excitation. Inset displays emission intensity as a function of pump energy density showing the slope of 1.99. Test environment: temperature of 25 °C, humidity of 55%.

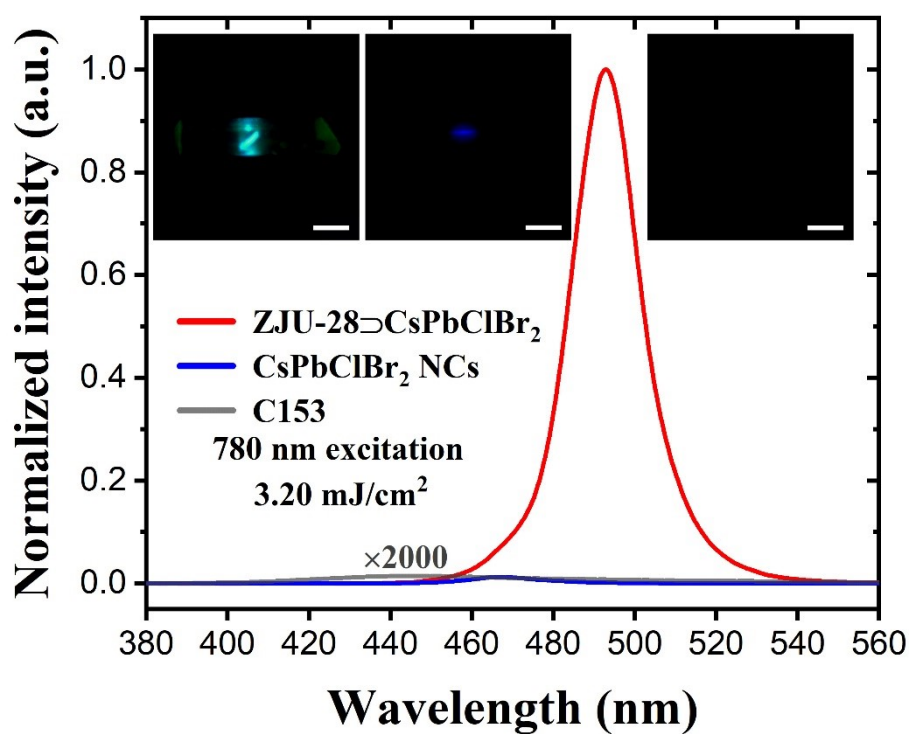


Fig. S30. Comparison of the 2PE luminescence at 780 nm from ZJU-28@CsPbClBr₂, CsPbClBr₂ NCs and Coumarin 153 under the same single pulse excitation fluence of 3.20 mJ/cm². Insets: the microscopy images of ZJU-28@CsPbClBr₂ (left), CsPbClBr₂ NCs (middle) and Coumarin 153 (right) under 780 nm excitation. Test environment: temperature of 25 °C, humidity of 55%.

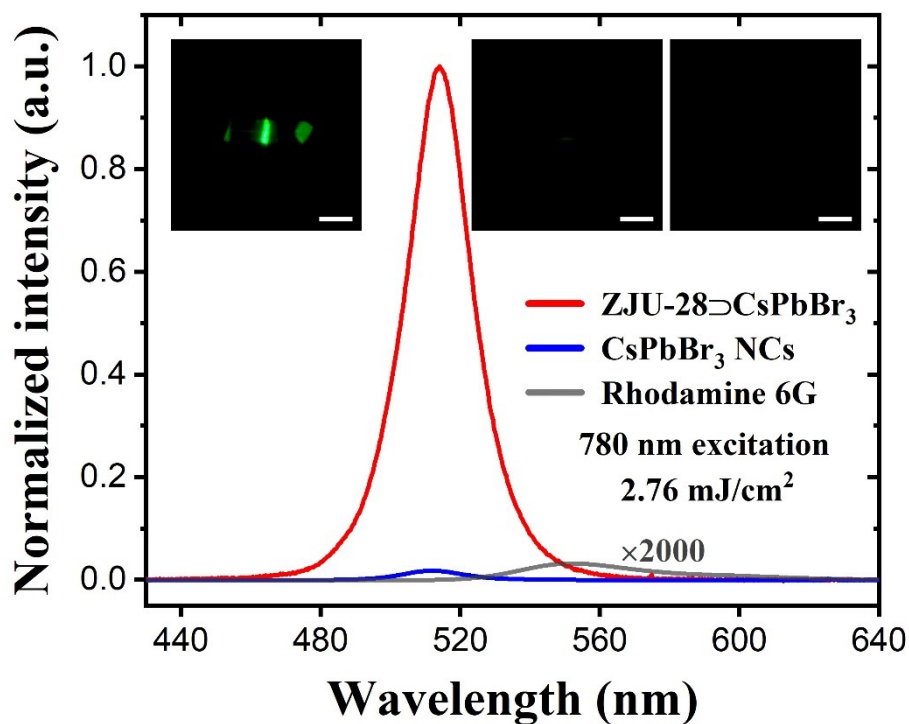


Fig. S31. Comparison of the 2PE luminescence at 780 nm from ZJU-28@CsPbBr₃, CsPbBr₃ NCs and Rhodamine 6G under the same single pulse excitation fluence of 2.76 mJ/cm². Insets: the microscopy images of ZJU-28@CsPbBr₃ (left), CsPbBr₃ NCs (middle) and Rhodamine 6G (right) under 780 nm excitation. Test environment: temperature of 25 °C, humidity of 55%.

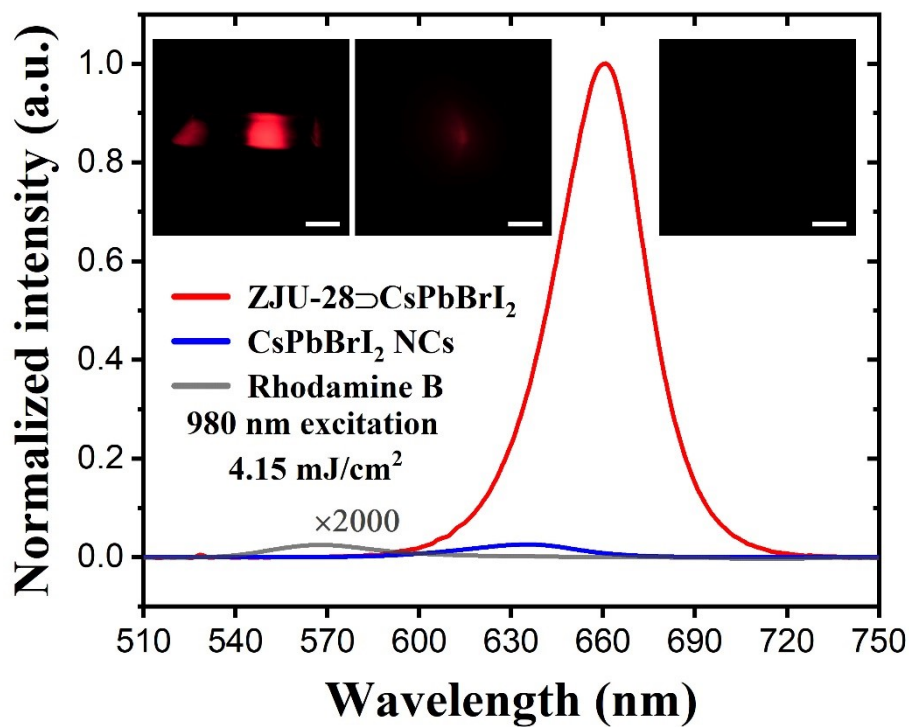


Fig. S32. Comparison of the 2PE luminescence at 980 nm from ZJU-28@CsPbBr₂, CsPbBr₂ NCs and Rhodamine B under the same single pulse excitation fluence of 4.15 mJ/cm². Insets: the microscopy images of ZJU-28@CsPbBr₂ (left), CsPbBr₂ NCs (middle) and Rhodamine B (right) under 980 nm excitation. Scale bar, 50 μm. Test environment: temperature of 25 °C, humidity of 55%.

Table S2. The comparison of 2PA cross-sections σ_2 and two-photon action cross-sections $\eta\sigma_2$ from ZJU-28 \supset CsPbX₃ crystals and CsPbX₃ NCs.

Materials	Conditions	2PA cross-section (GM)	Two-photon $\eta\sigma_2$ (GM)
ZJU \supset 28 \supset CsPbClBr ₂	~ 8.3 nm size, sphere, ~138 μ M in ZJU-28, at 780 nm, this work	~ 1.11 \times 10 ⁶	~ 0.22 \times 10 ⁶
CsPbClBr ₂ NCs	~ 9.2 nm size, cubic, ~ 1.6 μ M in toluene, at 780 nm, this work	~ 0.69 \times 10 ⁶	~ 0.22 \times 10 ⁶
	~ 12.4 nm size, cubic, 12-20 μ M in n-hexane, at 800 nm ⁹	~ 0.16 \times 10 ⁶	
ZJU-28 \supset CsPbBr ₃	~ 9.1 nm size, sphere, ~ 111 μ M in ZJU-28, at 780 nm, this work	~ 5.85 \times 10 ⁶	~ 1.58 \times 10 ⁶
	~ 9.3 nm size, cubic, ~ 1.7 μ M in toluene, at 780 nm, this work	~ 2.34 \times 10 ⁶	~ 1.45 \times 10 ⁶
CsPbBr ₃ NCs	~ 9 nm size, cubic, ~ 34 μ M in toluene, at 800 nm ¹⁰	~ 0.12 \times 10 ⁶	
	~ 9 nm size, cubic, ~ 2 μ M in toluene, at 800 nm ¹¹	~ 2.7 \times 10 ⁶	~ 1.62 \times 10 ⁶
	~ 9 nm size, cubic, ~ 1 μ M in toluene, 780 nm ¹²	~ 3.2 \times 10 ⁶	~ 1.8 \times 10 ⁶
ZJU-28 \supset CsPbBrI ₂	~ 12.5 nm size, sphere, ~ 39 μ M in ZJU-28, at 980 nm, this work	~ 2.62 \times 10 ⁶	~ 0.50 \times 10 ⁶
CsPbBrI ₂ NCs	~ 11.3 nm size, cubic, ~ 0.98 μ M in toluene, at 980 nm, this work	~ 0.77 \times 10 ⁶	~ 0.60 \times 10 ⁶
	~ 12.4 nm size, cubic, 12-20 μ M in n-hexane, at 800 nm ⁹	~ 0.26 \times 10 ⁶	

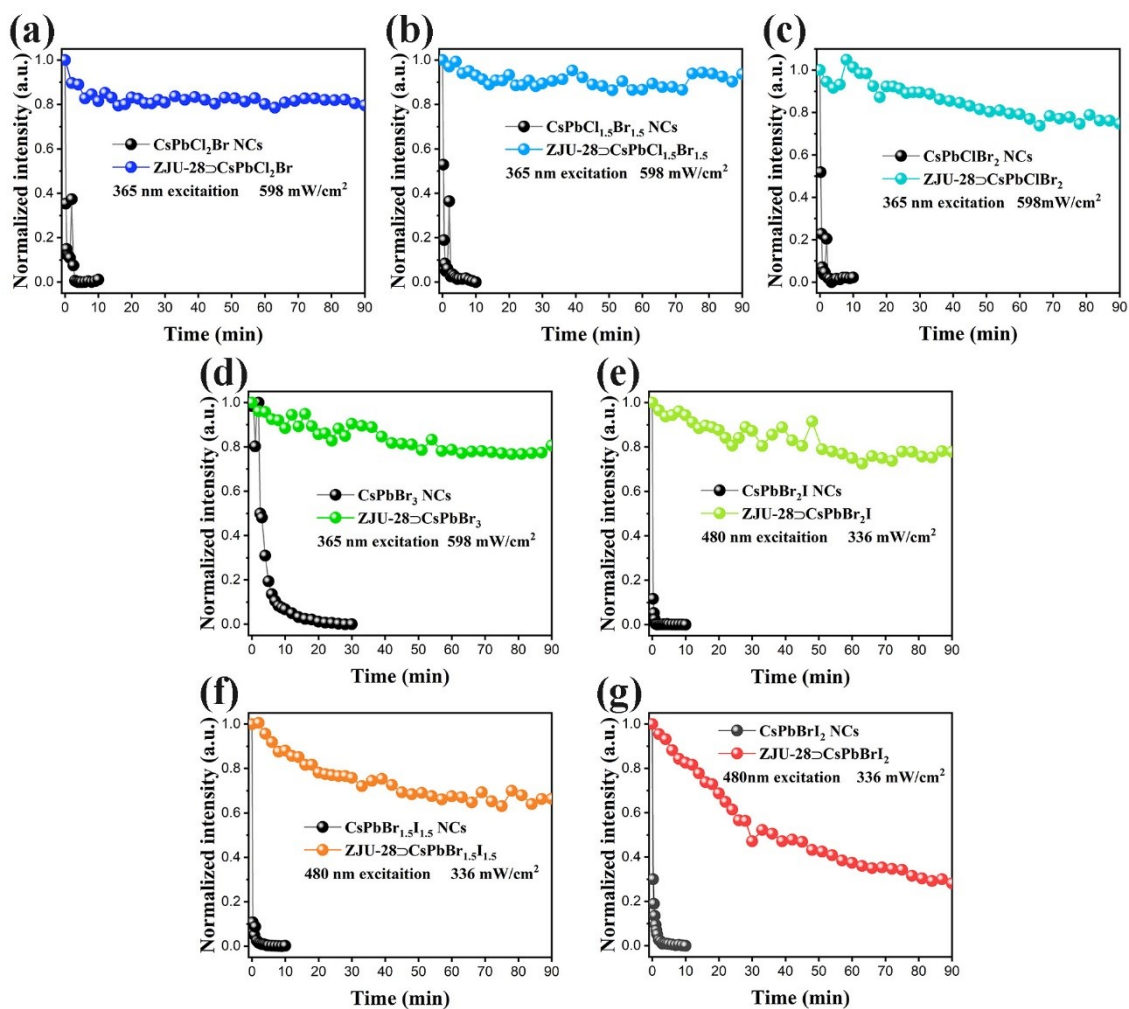


Fig. S33. Plots of relative PL intensity of an isolated ZJU-28 \rightarrow CsPbX₃ microcrystal and corresponding colloidal perovskite NCs under excitation of 365 nm or 480 nm as a function of irradiation time. (X₃ = (a) Cl₂Br, (b) Cl_{1.5}Br_{1.5}, (c) ClBr₂, (d) Br₃, (e) Br₂I, (f) Br_{1.5}I_{1.5} and (g) BrI₂). Test environment: temperature of 25 °C, humidity of 55%.

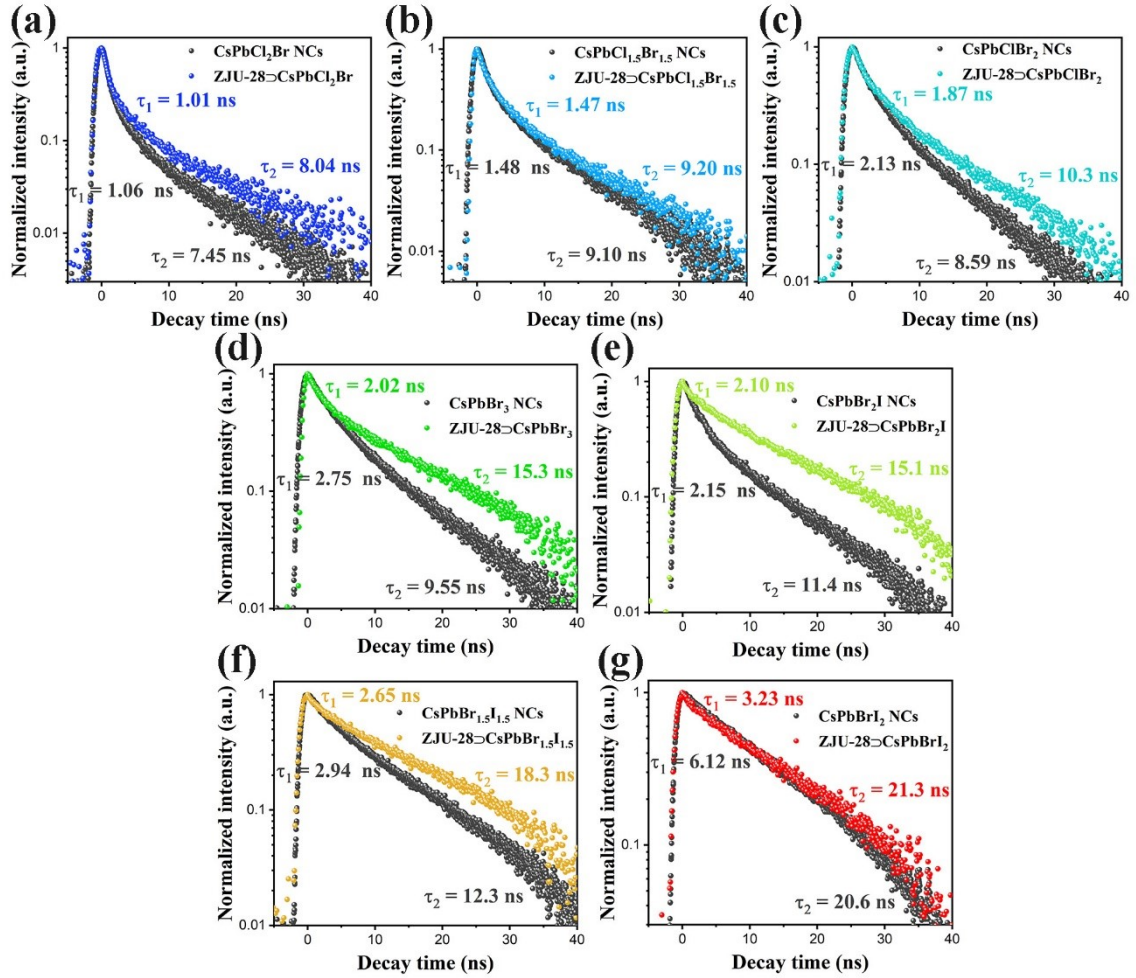


Fig. S34. Time-resolved PL decays of ZJU-28 CsPbX₃ crystals and corresponding CsPbX₃ NCs (X₃ = (a) Cl₂Br, (b) Cl_{1.5}Br_{1.5}, (c) ClBr₂, (d) Br₃, (e) Br₂I, (f) Br_{1.5}I_{1.5} and (g) BrI₂).

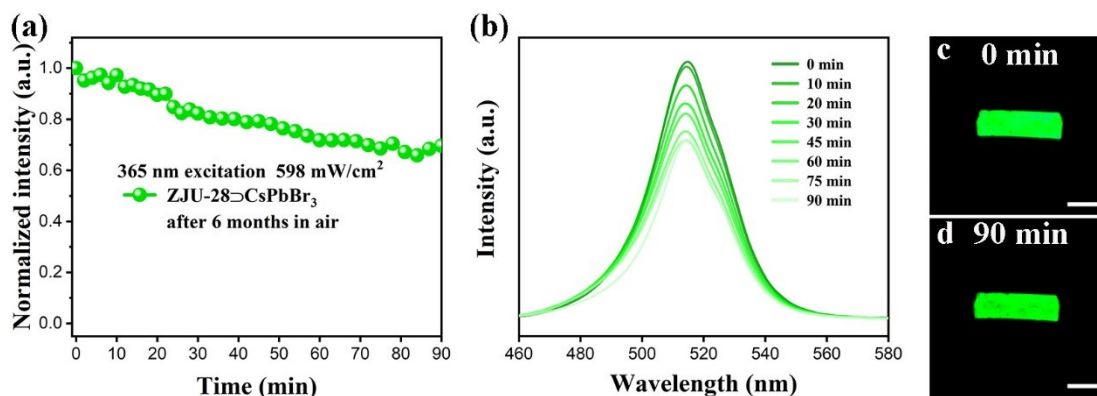


Fig. S35. (a) illumination-time-dependent luminescence intensity spectrum of an isolated ZJU-28 CsPbBr₃ microcrystal after stored in the air without additional protection for 6 months. (b) PL spectra changes of an isolated ZJU-28 CsPbBr₃ microcrystal under excitation of 365 nm for different time periods. The microscopy images of an isolated ZJU-28 CsPbBr₃ microcrystal after (c) 0 min and 90 min irradiation of 365 nm. Test environment: temperature of 25 °C, humidity of 55%.

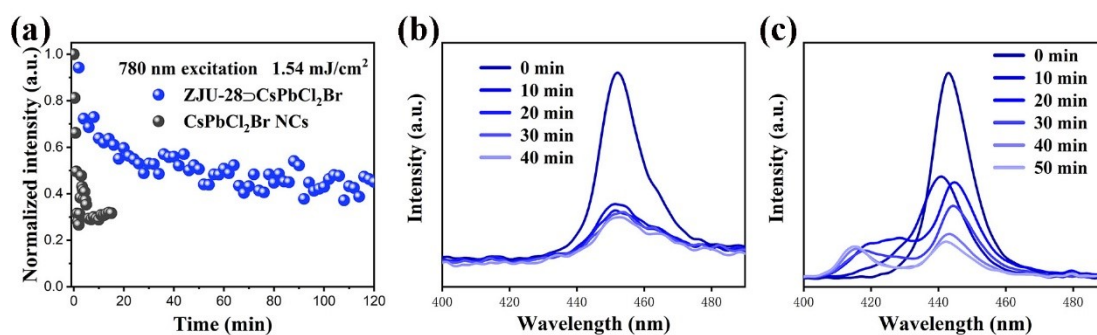


Fig. S36. (a) Plots of relative PL intensity of an isolated ZJU-28 CsPbCl₂Br microcrystal and CsPbCl₂Br NCs under fs laser excitation as a function of irradiation time. PL spectra changes of an isolated (b) ZJU-28 CsPbCl₂Br microcrystal and (c) CsPbCl₂Br NCs under 780 nm excitation for different time periods.

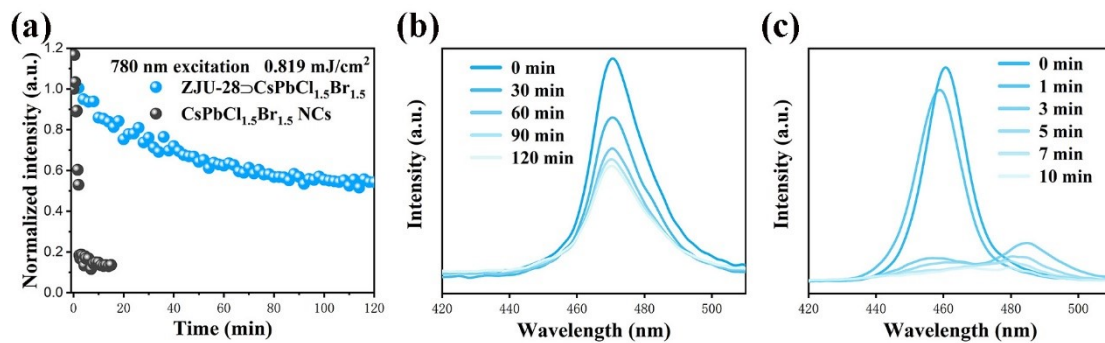


Fig. S37. (a) Plots of relative PL intensity of an isolated ZJU-28 CsPbCl_{1.5}Br_{1.5} microcrystal and CsPbCl_{1.5}Br_{1.5} NCs under fs laser excitation as a function of irradiation time. PL spectra changes of an isolated (b) ZJU-28 CsPbCl_{1.5}Br_{1.5} microcrystal and (c) CsPbCl_{1.5}Br_{1.5} NCs under 780 nm excitation for different time periods.

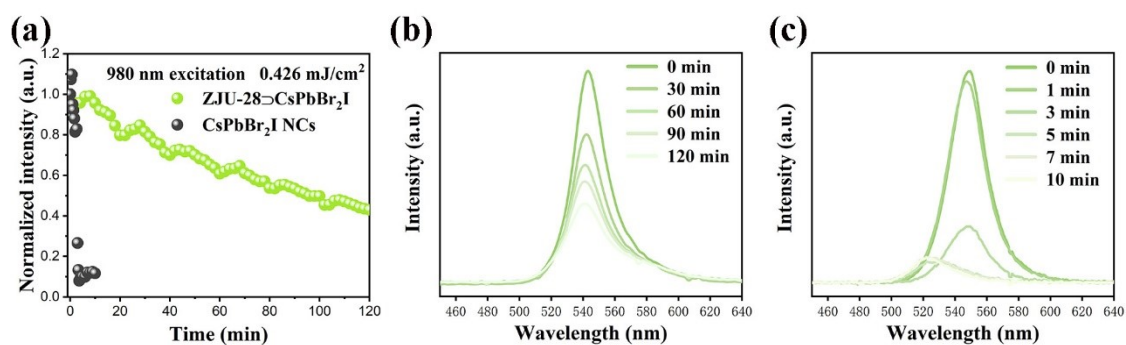


Fig. S38. (a) Plots of relative PL intensity of an isolated ZJU-28 CsPbBr₂I microcrystal and CsPbBr₂I NCs under fs laser excitation as a function of irradiation time. PL spectra changes of an isolated (b) ZJU-28 CsPbBr₂I microcrystal and (c) CsPbBr₂I NCs under 980 nm excitation for different time periods.

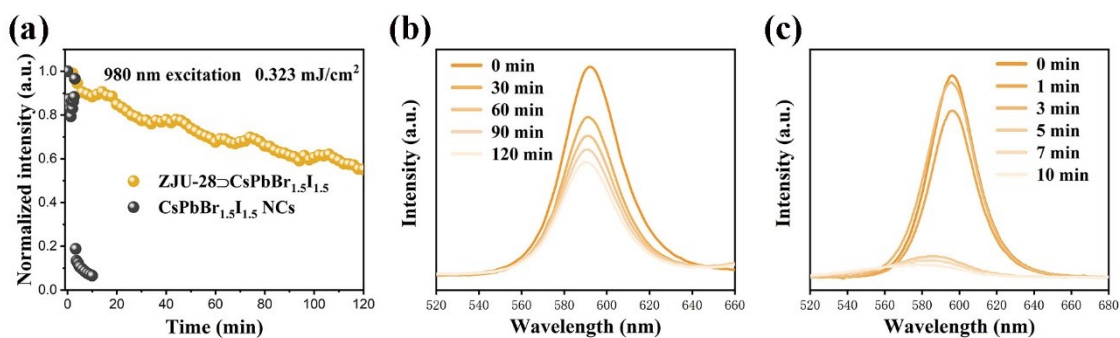


Fig. S39. (a) Plots of relative PL intensity of an isolated ZJU-28⊃CsPbBr_{1.5}I_{1.5} microcrystal and CsPbBr_{1.5}I_{1.5} NCs under fs laser excitation as a function of irradiation time. PL spectra changes of an isolated (b) ZJU-28⊃CsPbBr_{1.5}I_{1.5} microcrystal and (c) CsPbBr_{1.5}I_{1.5} NCs under 980 nm excitation for different time periods.

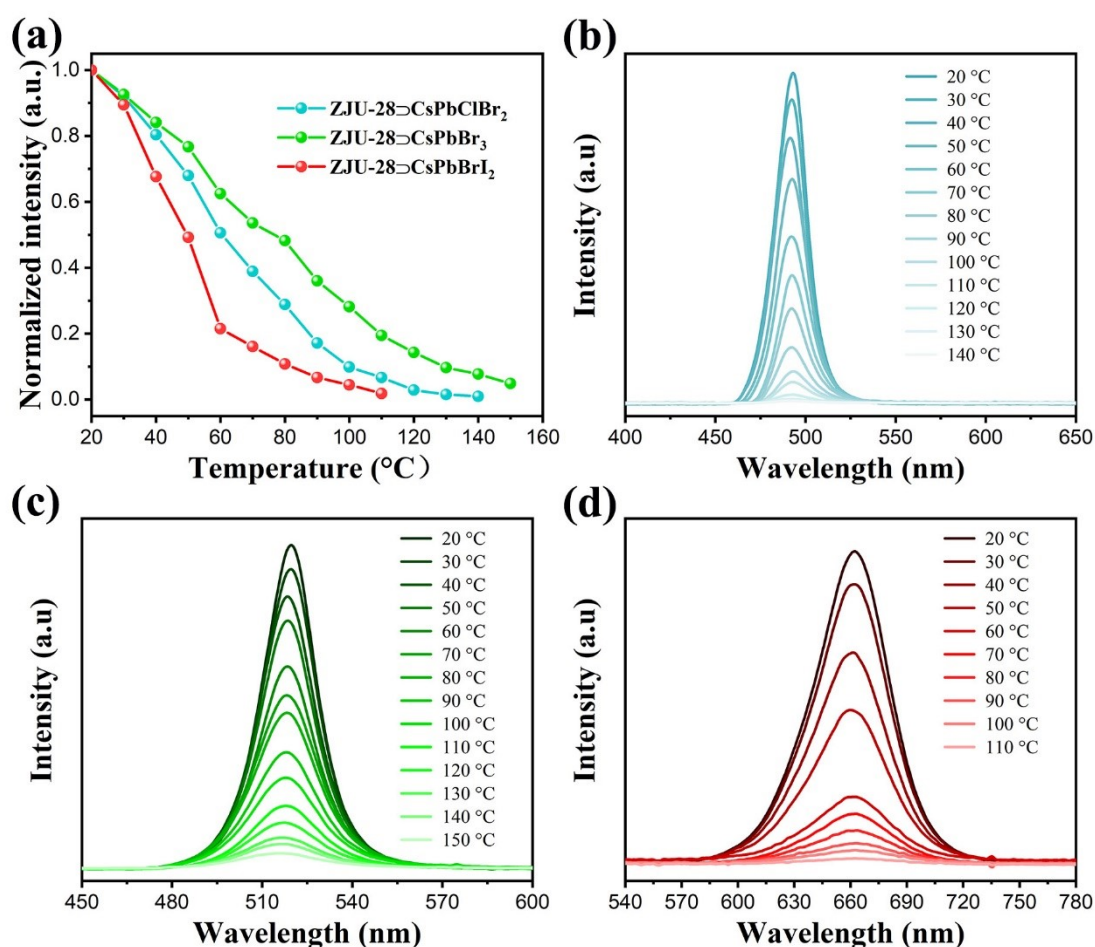


Fig. S40. The thermal stability of ZJU-28 \supset CsPbX₃ crystals. (a) Temperature-dependent normalized PL intensity of ZJU-28 \supset CsPbClBr₂, ZJU-28 \supset CsPbBr₃ and ZJU-28 \supset CsPbBrI₂. Thermal stability test of (b) ZJU-28 \supset CsPbClBr₂, (c) ZJU-28 \supset CsPbBr₃ and (d) ZJU-28 \supset CsPbBrI₂. Test environment: humidity of 50% and in air.

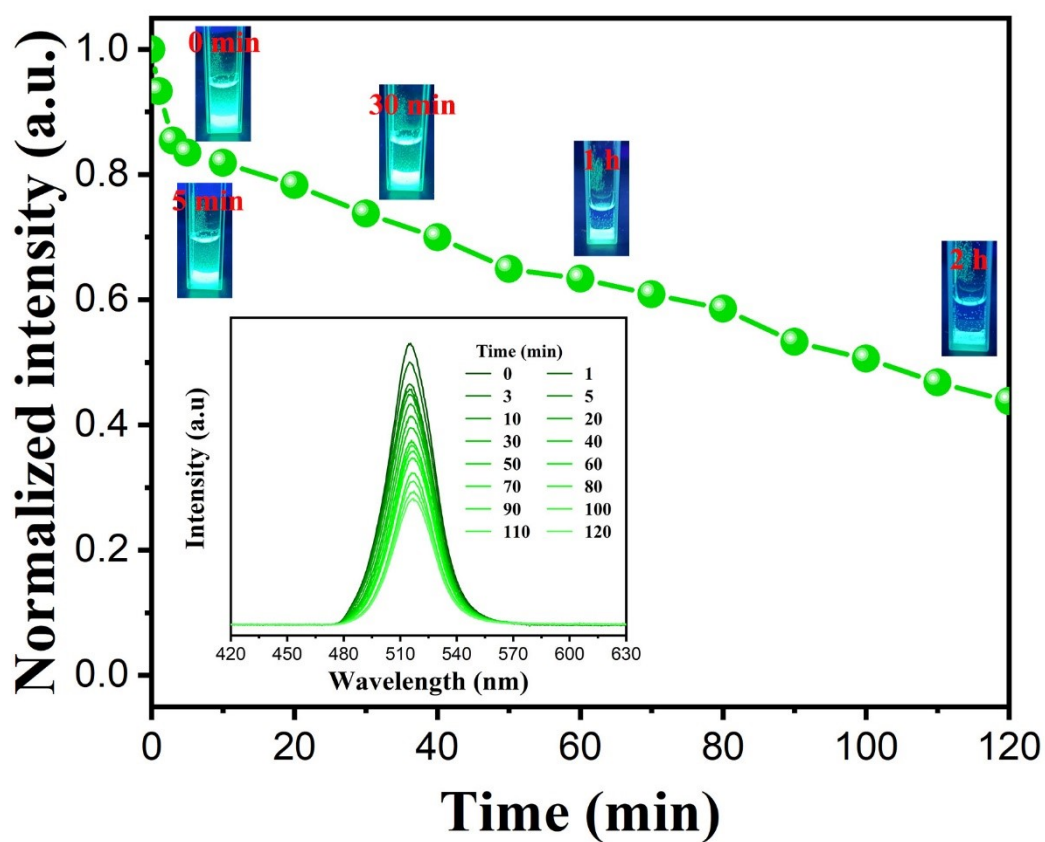


Fig. S41. Time-dependent normalized PL intensity of ZJU-28 \supset CsPbBr₃ after immersed into

water. Insets: PL spectra changes of ZJU-28 \rhd CsPbBr₃ for different time periods of immersion and corresponding photographs. Test environment: temperature of 25 °C, humidity of 55%.

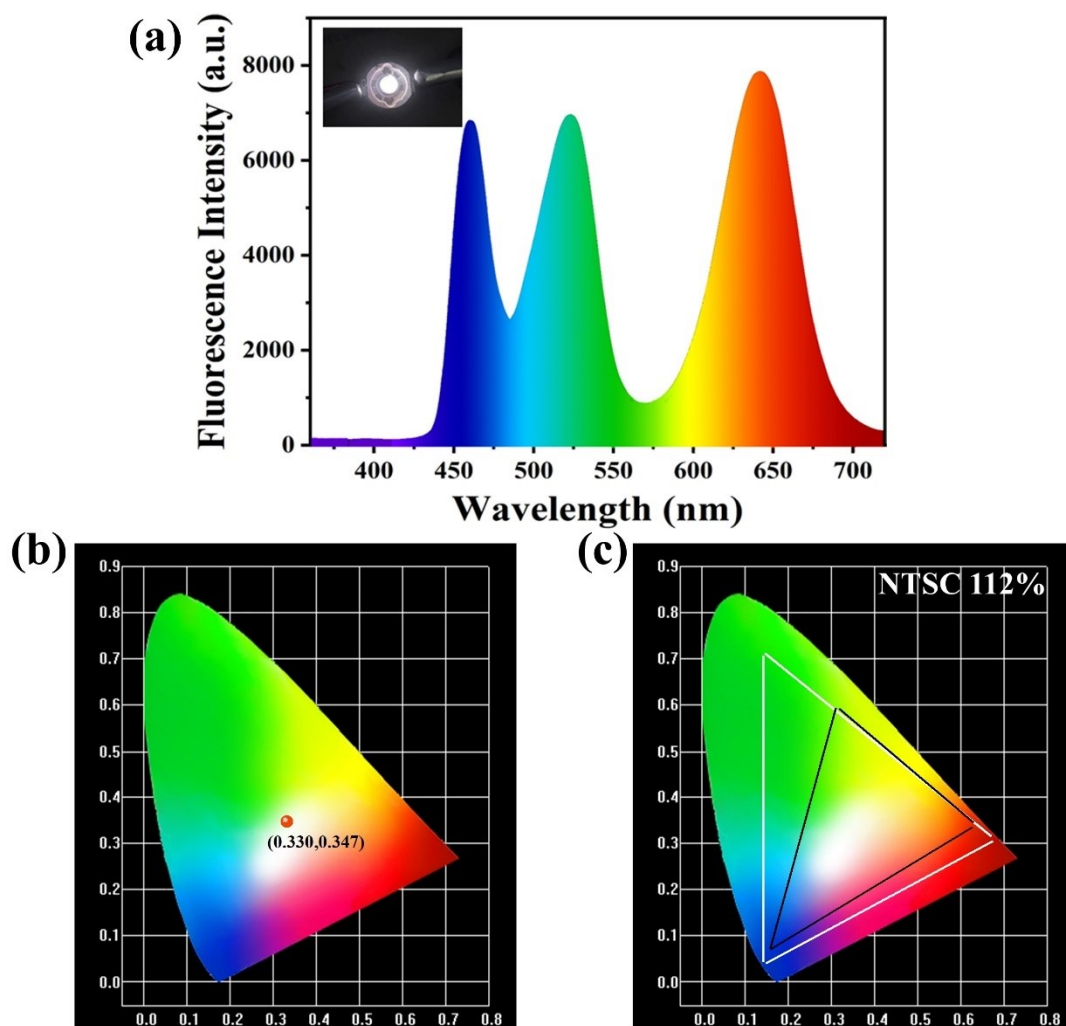


Fig. S42. (a) The emission spectrum and (b) CIE color coordinates of the LED device constructed by combining UV chip, ZJU-28 \rhd CsPbBr₃ crystals and ZJU-28 \rhd CsPbBr₂ crystals, (c) Comparison of the obtained NTSC display gamut (the area shown by the white line) with the 72% NTSC standard gamut (the area shown by the black line).

4. References

- 1 J. Yu, Y. Cui, C. Wu, Y. Yang, Z. Wang, M. O'Keeffe, B. Chen and G. Qian, *Angew. Chem., Int. Ed.*, 2012, **51**, 10542.
- 2 L. Protesescu, S. Yakunin, M. I. Bodnarchuk, F. Krieg, R. Caputo, C. H. Hendon, R. X. Yang, A. Walsh and M. V. Kovalenko, *Nano Lett.*, 2015, **15**, 3692.
- 3 H. He, Y. Cui, B. Li, B. Wang, C. Jin, J. Yu, L. Yao, Y. Yang, B. Chen and G. Qian, *Adv. Mater.*, 2019, **31**, 1806897.
- 4 R. Medishetty, J. K. Zareba, D. Mayer, M. Samoc and R. A. Fischer, *Chem. Soc. Rev.*, 2017, **46**, 4976.
- 5 G. Jones II, W. R. Jackson, C. Choi, W. R. Bergmark, *J. Phys. Chem.*, 1985, **89**, 294.
- 6 N. S. Makarov¹, M. Drobizhev¹, A. Rebane, *Opt. Express*, 2008, **16**, 4029.
- 7 L. S. Rohwer and J. E. Martin, *J. Lumines.*, 2005, **115**, 77.
- 8 P. C. Beaumont, D. G. Johnson, B. J. Parsons, *J. Chem. Soc. Faraday Trans.*, 1993, **89**, 4185.
- 9 Q. Han, W. Wu, W. Liu, Q. Yang and Y. Yang, *Opt. Mater.*, 2018, **75**, 880.
- 10 Y. Wang, X. Li, X. Zhao, L. Xiao, H. Zeng and H. Sun, *Nano Lett.*, 2016, **16**, 448.
- 11 Y. Xu, Q. Chen, C. Zhang, R. Wang, H. Wu, X. Zhang, G. Xing, W. W. Yu, X. Wang, Y. Zhang and M. Xiao, *J. Am. Chem. Soc.*, 2016, **138**, 3761.
- 12 W. Chen, S. Bhaumik, S. A. Veldhuis, G. Xing, Q. Xu, M. Grätzel, S. Mhaisalkar, N. Mathews and T. C. Sum, *Nat. Commun.*, 2017, **8**, 15198.